Research Article

Tuning of ferrites ($Co_xFe_{3-x}O_4$) nanoparticles by co-precipitation technique

R. Sagayaraj[1] · S. Aravazhi[2] · C. Selva kumar[2] · S. Senthil kumar[2] · G. Chandrasekaran[3]

Abstract
The synthesis of cobalt ferrites ($Co_xFe_{3-x}O_4$) materials with sympathetic size and tunable magnetic properties is used for the promising industrial and biomedical applications. Such cobalt ferrites nanoparticles have been employed by co-precipitation technique. XRD analysis revealed that the average crystallite size of synthesized powder is 9 nm using (311) peaks, and it has exhibited polycrystalline structure. FTIR spectroscopy showed the formation of ferrite phase with high- and low-frequency bands at 573 cm^{-1} and 455 cm^{-1}, respectively. The TEM images exposed that the materials have been well agglomerated along with spherical-shaped nanoparticles. EDX study confirmed the presence Co, O, Fe and C with stoichiometric composition and no more impurity detected in the spectrum. The VSM analysis revealed that the sample exhibits the hard magnetic materials. In addition, the magnetic anisotropy increases (19.05 → 344.84 erg/g) when Co is added with Fe_3O_4. EPR spectroscopy confirmed the ferromagnetic behavior of composites.

Keywords Cobalt ferrites · Co-precipitation · Spherical shape · Polycrystalline · Magnetic anisotropy · EPR spectroscopy

1 Introduction

Nowadays, nonpolluting vehicles have been constructed using advanced magnetic spinel materials. The cobalt ferrites were formed by face-centered cubic structure through oxygen ions filled together with the divalent and trivalent metal ions in the tetrahedral and octahedral voids, respectively. Cobalt ferrite ($CoFe_2O_4$) nanocomposites are broadly used in a variety of applications, such as transformer cores, magnetic sensors, stress and biomedical sensors, catalytic insulators, information and energy storage media, solar energy conversion, coatings, recording heads, antenna rods, loading coils, microwave devices, ferrofluids, magnetic refrigeration, drug delivery, gas detectors, cellular therapy, tissue repair and hyperthermia treatment. Cobalt ferrite spinel is a promising material for various commercial applications [1, 2]. For materials calcined at 900 °C, there is a slight move of the 311 peak toward lower edges, credited to the migration of Co^{2+} cations from octahedral to tetrahedral voids and to a contrary exchange of a proportional number of Fe^{3+} particles so as to loosen up the compressive strain. It demonstrates the variety of crystallite sizes and lattice parameters with $CoFe_2O_4$ content (X %). By calcining temperature, at 700 °C, the evaluated lattice parameters of $CoFe_2O_4$ are underneath the theoretical value (8.39 Å) as per JCPDS NO. 22-1086, because of the progressions of Co^{2+} and Fe^{3+} cations circulation among tetrahedral and octahedral destinations. In cobalt ferrite structure, Fe^{3+} and Co^{2+} can possess both tetrahedral and octahedral sites [3, 4]. The exchange of cations framework is said to be a spinel structure. Normally, cobalt ferrites ($CoFe_2O_4$) exist in the spinel oxide family and every unit cell containing $32O^{2-}$, $8Co^{2+}$ and Fe^{3+} ions. The cobalt ferrite molecule framed the Fe^{3+} $[Co^{2+}Fe^{3+}]$ O^{2-}; here, Fe^{3+} cations occupy half of the

✉ R. Sagayaraj, sagayarajnancy@gmail.com | [1]PG & Research Department of Physics, St. Joseph's College of Arts and Science (Autonomous), Cuddalore, Tamilnadu 607001, India. [2]Department of Physics, Arignar Anna Arts College, Villupuram, Tamilnadu 605602, India. [3]Department of Physics, Pondicherry University, Pondicherry 605014, India.

SN Applied Sciences (2019) 1:271 | https://doi.org/10.1007/s42452-019-0244-7

Received: 14 September 2018 / Accepted: 11 February 2019 / Published online: 27 February 2019

octahedral fashion and tetrahedral fashion. $CoFe_2O_4$ is an example of an inverse spinel structure [5–9]. In view of its high magnetocrystalline anisotropy, saturation magnetization, high coercivity, substance soundness, mechanical hardness and chemical stability, cobalt ferrite ($CoFe_2O_4$) spinel is a promising material for different business applications. Its magnetic properties are for the most part dictated by the Co^{2+}, and along these lines, the tuning of its magnetic characters by modifying the Co/Fe proportion ends up conceivably. By warm treatment, the $Co_xFe_{3-x}O_4$ is gradually changed in two iron-rich and cobalt-rich spinel stages [10]. For the gel that contains a high abundance of Co, the hysteresis loop demonstrates expansive coercive field, yet the magnetic subsidiary outline exhibits sharp peaks, conceivable as a result of the existence of $CoFe_2O_4$ as a single magnetic phase. In favor of samples calcined at 700 °C, the saturation magnetization declines, and the decline pattern of the saturation magnetization could be a result of the diverse cation distribution [11].The exchange of the different cations in the spinel matrix is responsible for the fascinating magnetic performance of the different ferrites [12]. These magnetic cations were exchanged between the voids in various experimental methods, and also an exchange of cations depends on doping materials, annealing temperature and duration of time [13]. Magnetic cobalt ferrites have been synthesized by a variety of methods, such as mechanical milling, co-precipitation, hydrothermal methods and sol–gel techniques. Among this, co-precipitation is the most convenient technique when compared to others by controlling the size of the nano particles [14]. The polyvinylpyrrolidone (PVP) is added with $CoFe_2O_4$ as a stabilizer [15]. These ferrite materials have been widely used in various technical applications in magnetic refrigeration, detoxification of biological fluids, magnetically controlled transport of anticancer drugs, magnetic resonance imaging contrast enhancement, magnetic cell separator, magnetic devices, switching devices, permanent magnets, hard disk, recording media, read–write heads, active component of ferrofluids, color imaging, gas-sensitive materials, etc. [16–19].In the present work, a novel co-precipitation technique is utilized for the arrangement of $Co_xFe_{3-x}O_4$ nanoferrites. The reactants utilized are modest, nonlethal and eco-accommodating. The grain sizes of the arranged ferrites are in the request of a couple of nanosizes. The combined ferrites are checked for their virtue and organization. The nanoferrites are found to have high caliber and great stoichiometric piece which purifies the inclination of this technique.

2 Experimental section

2.1 Materials

Ferric sulfate monohydrate ($Fe_2(SO_4)_3.H_2O$, assay: 99%),cobalt (II) sulfate heptahydrate ($CoSO_4.7H_2O$), ethanol, ammonia, polyvinyl pyrrolidone (PVP, $(C_6H_9NO)_n$, assay: 98%) were purchased from Sigma-Aldrich Chemical company. All chemicals are used without any further purification.

2.2 Synthesis of PVP-coated $Co_xFe_{3-x}O_4$ nanoparticles

Nanoscale particles were prepared by chemical co-precipitation method. The number of moles of all reagents of sample and the corresponding chemical formula are shown in Table 1. In an experiment, aqueous solutions of 100 ml containing the ferric sulfate, cobalt (II) sulfate heptahydrate (x: $0.00 \le x \le 0.04$), respectively, and polyvinyl pyrrolidone (PVP = 0.0025M = 1 g) were mixed with 250-ml conical flask with stoichiometric proportion. The stoichiometric mixtures were stirred for 45 min to obtain a homogeneous solution, and the ammonia (0.25 M) was dissolved in 50 ml of distilled water and added slowly to the mixtures for maintaining the pH level at 11 of materials. Under vigorous mechanical stirring for 3 h at room temperature, the solution appears in black color; this is the required condition for precipitation of the nanoparticles. The precipitates were then magnetically alienated using a magnet bar. The alienated materials were dissolved in methanol and then again alienated with magnet bar. This process was continuously done for four times in order to eliminate the excess amine molecules. Finally, we got a black powder of $CoFe_2O_4$ after drying the precipitate at room temperature for 6 h. The dried powder was kept at muffle furnace and annealed at 600 °C for 4 h in order to obtain pure-phase high-crystallinity $CoFe_2O_4$ ferrites. Therefore, annealing operation removes all structural imperfections by complete recrystallization.

Table 1 The number of moles of all reagents of $Co_xFe_{3-x}O_4$ nanoparticles with x: $0.00M \le x \le 0.04M$

S. no	Reagent ($Co_xFe_{3-x}O_4$)	Mole
1	$Fe_2(SO_4)_3.H_2O$	3 M
2	$CoSO_4.7H_2O$	x: $0.00M \le x \le 0.04M$
3	NH_3	0.25M
4	PVP	0.0025M = 1 g

3 Results and discussion

3.1 XRD analysis

We used the officially announced [20] XRD spectrum Fe_3O_4 for correlation in the succeeding employment. The chemical composition, nanosize, lattice constant, X-ray density, volume of unit cell and micro-strain are summarized in Table 2. The XRD patterns of $Co_xFe_{3-x}O_4$ (where *x*: $0.00 \le x \le 0.04$) are shown in Fig. 1. From the XRD graph, it is confirmed that no extra peaks of impurity are present in the crystalline microstructure. On adding 'Co' with Fe_3O_4, it affects domain structure and improves its crystal parameters. Because cobalt cations promote the crystalline forms a spherical shape with peaks. The Co^{2+}(70 pm) ions at the tetrahedral sites are being replaced by Fe^{3+} ions (60 pm) with significant ionic radius [21, 22]. The crystallite size decreases (19.2 → 5.53 nm) significantly when the annealing temperature is 600 °C with different doping ratios of Co^{+2} while the Fe^{3+} cations are shared in both voids. Now the sample performs as the inverse spinel structure [23]. All the observed peaks were indexed to cubic spinel structure using JCPDS data (Card No: 89–4307), and their reflections (220), (110), (311), (024), (422), (333) and (440) showed the construction of single-phase cubic inverse spinel structure. The crystallite size of $CoFe_2O_4$ nanoparticles is calculated by using Debye–Scherrer's formula [15, 24, 25]:

$$D = K\lambda/\beta \cos\theta$$

where *K* is the shape factor (0.9), λ is the wavelength of the X-ray (1.5406 Å), β is the full width at half maximum and θ is the Bragg angle. The average crystallite size of the sample is 9 nm using the (311) peak. The lattice constant was determined from XRD data by the following formula [26]:

$$a = d\left(h^2 + K^2 + l^2\right)^{1/2} \text{Å}$$

where '*a*' is the lattice constant, '*d*' is the interplanar spacing and (h k l) are Miller indices. The lattice constant shows the single phase and has the same value (8.35 Å) for their entire sample. The lattice constant of $Fe_{3M}O_4$ is 8.357 Å while increasing the mole ratio of Co^{2+} ions by 0.01M, 0.02M, 0.03M the lattice constant remains the same. The strain produced beyond 0.03M the lattice constant is slightly increased by 0.034 Å due to stress and strain on the surface of the materials are induced by PVP matrix [27]. As the Co^{2+} concentration rises, the structure will be more nearby to inverse spinel type that in turn reduces the contribution of hopping and decreases the size [9]. The X-ray density (D_x) was computed from the values of lattice parameter (a) using the following formula [28–31]:

$$D_x = 8M/Na^3 g/cm^3.$$

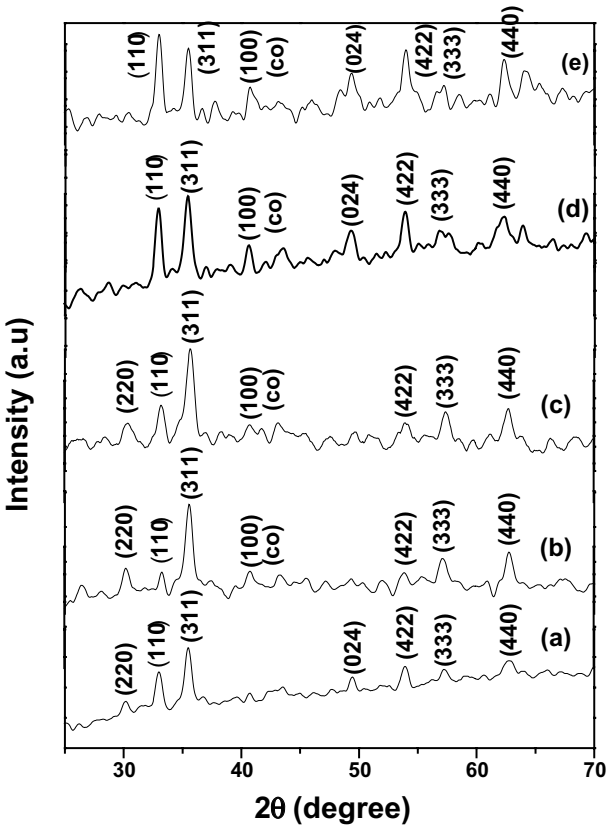

Fig. 1 X-ray diffraction of cobalt ferrite nanoparticles. **a** $Fe_{3M}O_4$, **b** $Co_{0.01M}$ $Fe_{2.99M}O_4$, **c** $Co_{0.02M}$ $Fe_{2.98M}O_4$, **d** $Co_{0.03M}$ $Fe_{2.97M}O_4$, **e** $Co_{0.04M}$ $Fe_{2.96M}O_4$

Table 2 Structural properties of ferrite nanoparticles (XRD)

Materials	Crystalline size (nm)	Lattice constant (a) Å	Lattice strain (ε)	Volume Å^3	X-ray density (g/cm$^{3)}$
$Fe_{3M}O_4$	13.2	8.357	0.009	583.6	5.34
$Co_{0.01M}$ $Fe_{2.99M}O_4$	19.2	8.357	0.006	583.6	5.34
$Co_{0.02M}$ $Fe_{2.98M}O_4$	5.8	8.357	0.020	583.6	5.34
$Co_{0.03M}$ $Fe_{2.97M}O_4$	5.8	8.357	0.020	583.6	5.34
$Co_{0.04M}$ $Fe_{2.96M}O_4$	5.7	8.391	0.020	590.8	5.27

where '8' represents the number of molecules in a unit cell of spinel lattice, '*M*' is the molecular weight of composition, '*N*' is the Avogadro's number and '*a*' is the lattice parameter. It can be seen from Table 2, the X-ray density (D_x) increases with the increasing Co substitution in Ni Ferrites and it shows the densification of the material. The X-ray density is found to depend on the lattice parameter and molecular weight of the samples. Hence, the substituted Co^{2+} increases, the lattice parameter decreases and X-ray density increases. The volume of the unit cell is [28]

$$V = a^3(\text{Å})^3.$$

The volume of the unit cell decreases with increasing Co substitution in Fe_3O_4, because the lattice parameter decreases by increasing the Co concentration. The strain induced in the grown nanoparticles has been calculated using the following formula [31]:

$$\varepsilon = (\beta \cos\theta)/4$$

where β is full width at half maximum measured in radians and θ in degrees. A micro-strain (lattice strain) means that the distance of the relevant crystal planes is not identical which is possibly due to the presence of defects and stress. Furthermore, the overall decrease of the lattice parameters occurred when the bigger ion (Co^{2+}→70 nm) is partially substituted by the smaller one (Fe^{3+}→60 nm).

3.2 FTIR analysis

To legitimize the presence of Co^{2+} particles in our tail compound, we think about the effectively detailed FTIR spectrum of pure Fe_3O_4 [20] for comparison as appeared in Fig. 2. FTIR spectroscopy is used to study the surface chemistry and different bonds existing in the nanoparticles [32]. The Fourier-transform infrared spectra of $CoFe_2O_4$ nanoparticles were recorded in the frequency range in between 400 and 4000 cm^{-1}. The subject of the absorption spectrum reveals that positions of the cations in the crystal through the vibration mode. The strong peaks about 573-538 cm^{-1} wave number were due to the stretching vibrations of the metal at the tetrahedral voids (Fe–O–Co) with the high-frequency bands, and the stretching vibrations of the metal complex (Fe–O–Fe) at the octahedral voids appear lower with frequency bands at 468-455 cm^{-1} which confirms the phase of $CoFe_2O_4$ [24, 32]. It helps to improve their magnetic property to have inverse spinel structures. The stretching of C–O bond at 1136 cm^{-1} [33] and 867 cm^{-1} was assigned to deformation of Fe–OH groups [34]. The peaks at 1594 cm^{-1} were assigned to stretching and bending vibrations of absorption water on surfaces of nanostructures [35]. The vibrational frequencies associated

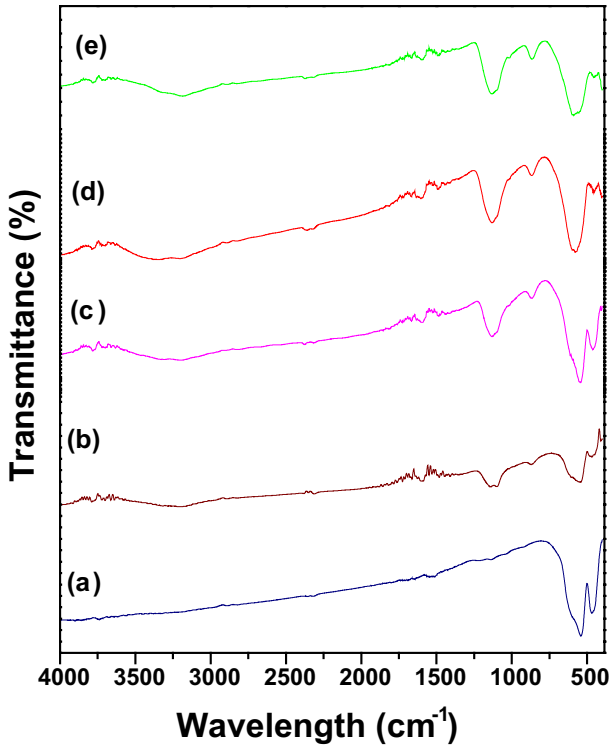

Fig. 2 FTIR spectra of cobalt ferrite nanoparticles. **a** $Fe_{3M}O_4$, **b** $Co_{0.01M}$, $Fe_{2.99M}O_4$, **c** $Co_{0.02M}$, $Fe_{2.98M}O_4$, **d** $Co_{0.03M}$ $Fe_{2.97M}O_4$, **e** $Co_{0.04M}$ $Fe_{2.96M}O_4$

with cobalt ferrite material centered at 3191 cm^{-1} are due to O–H stretching. The infrared absorption frequencies and the corresponding vibrational assignments of $CoFe_2O_4$ nanoparticles are shown in Table 3.

3.3 TEM analysis

Figure 3a–c shows the morphology of $Co_xFe_{3-x}O_4$ ($x = 0.03$ M) which was observed by a picture of TEM, correspondingly. The particle size is varied from 2 to 50 nm which is evident from our work reported [20] for Fe_3O_4 nanoparticles. The domain wall morphology has positively oriented domains that grow up, and the negatively oriented ones shrink. The nature of $CoFe_2O_4$ particles becomes regular, and the allotment of particles is uniform. The Co^{2+} cation is doped with Fe_3O_4 pure ferrites, and the nanoparticles achieved spherical shape and good agglomeration. Hence, the estimated particle size decreases from 100 to 2 nm. It reveals that the particles exhibited the super-ferromagnetic nature [16]. These nanosized particles form nanocluster in order to reduce the interfacial energy connecting the personage nanocrystals with the desired size of particles and are used in drug delivery applications [17]. The patterns of selective area electron diffraction (SAED) of the samples are shown in Fig. 3d. The

Table 3 Tentative vibrational assignments of ferrite nanostructures

Frequencies (cm^{-1})					Tentative vibrational assignments
$Fe_{3M}O_4$	$Co_{0.01M}Fe_{2.99M}O_4$	$Co_{0.02M}Fe_{2.98M}O_4$	$Co_{0.03M}Fe_{2.97M}O_4$	$Co_{0.04M}Fe_{2.96M}O_4$	
–	–	–	–	3191	O–H stretching
–	–	–	1594	1594	Stretching and bending vibrations of absorption water on surfaces nanostructures
–	1126	1136	1126	1126	Stretching of C–O bond
–	–	867	867	867	Fe–OH groups
538	538	538	573	573	Tetrahedral clusters intrinsic stretching vibrations of the metal at the tetrahedral site (C_O↔Fe) high-frequency bonds
468	468	455	455	468	Octahedral clusters assigned to octahedral-metal stretching (Fe↔Fe) low-frequency bonds

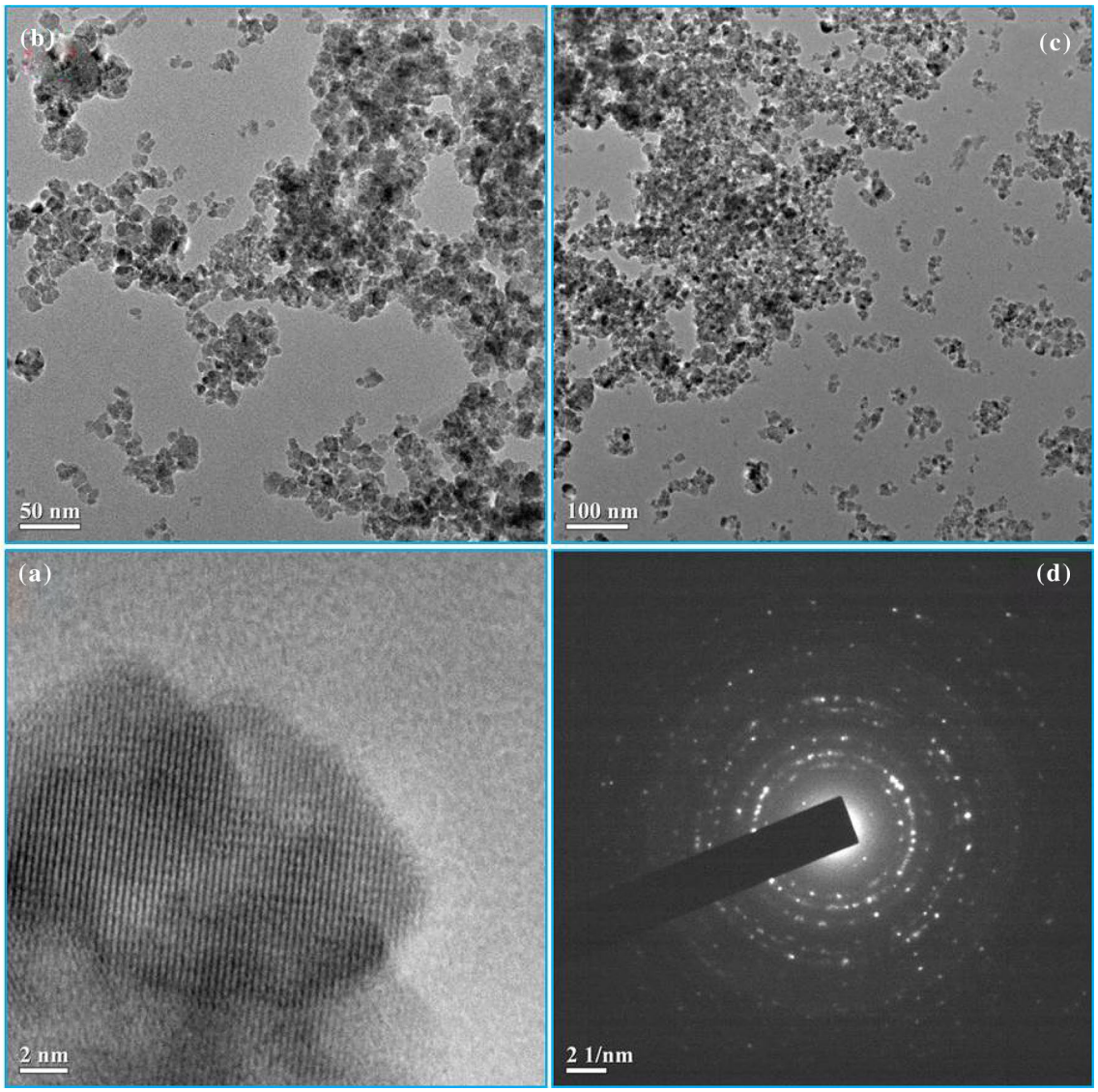

Fig. 3 TEM images (**a**–**c**) and SAED pattern (**d**) of $Co_{0.03M}Fe_{2.97M}O_4$ nanoparticles

polycrystalline nature of a pure $CoFe_2O_4$ with high crystallinity is revealed. And the bright spot is also obtained with Debye ring pattern which represents polycrystalline nature of the samples. Chemical purity along with stoichiometry of the $CoFe_2O_4$ nanoparticles was examined by EDX spectroscopy. We found that Co, Fe, C, O elements alone are present in the sample as shown in Fig. 4. The EDX study also confirmed that the precursors used in the synthesis have entirely undergone the chemical effect to form the single-phase nanocrystalline cobalt ferrite.

3.4 VSM analysis

The VSM analysis of $Co_xFe_{3-x}O_4$ (where $x = 0.03$ M) is shown in Fig. 5. The sample of $Co_{0.03M}Fe_{2.97M}O_4$ shows the enormous changes in magnetic specifications, when compared to Fe_3O_4 nanoparticles [20] which are synthesized by precipitation method. The hysteresis loops were identified and characterized to clarify the parameters of ferromagnetic materials, such as the saturation magnetization (M_s), retentivity (M_r) and coercivity (H_{ci}). The magnetic factors for the materials are prepared by co-precipitation methods as summarized in Table 4. For the site occupancy of magnetic cations at the tetrahedral along with octahedral sites define magnetization (M_s) [16]. The magnetic ability of spinel ferrites is actively dependent on the share of the various cations among (*A*) and (*B*) sites [17]. The Co^{2+}–O^{2-}–Fe^{3+} exchange interaction is very strong. So, these pairs of metal ions (radical's production: two or more atoms bound together as a single unit and form part of a domain) were contributing magnetic energy, whereas the Fe^{3+}–O^{2-}–Fe^{3+} interaction is very weak because Fe^{3+} ions were antiferromagnetically (↑↓) coupled. Hence, theses pair of metal ions cannot contribute magnetic energy in the sample [36]. This involves that the hysteresis loop of the materials was exaggerated evidently by doped elements at the room temperature, The saturation magnetization was decreased from 10.064E−3 to 0.5008 emu/g, but the residual magnetization and coercivity of ferrite were endorsed of the cobalt ferrite [21]. The ionic radius of Co^{2+} (70 pm) is greater than Fe^{3+} (60 pm) cation. Hence, Fe^{+3} cations are shared

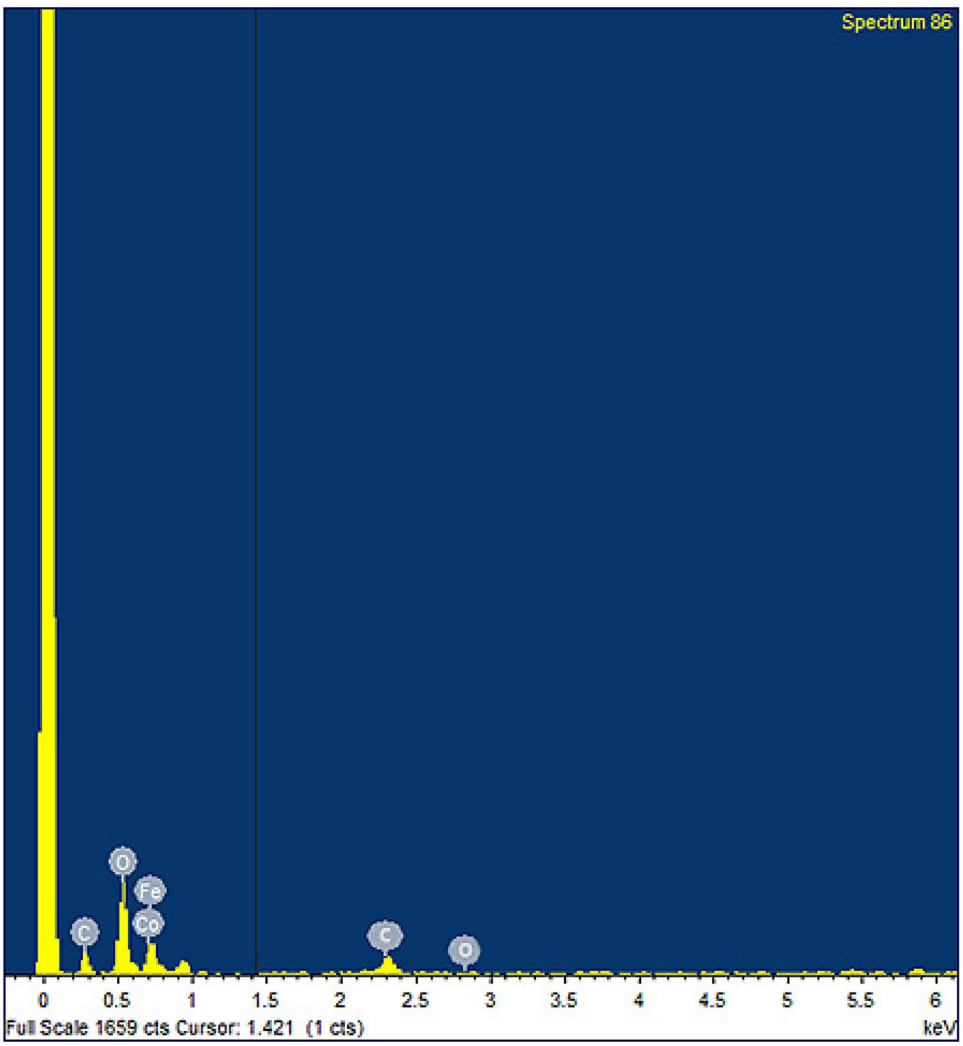

Fig. 4 Energy-dispersive analysis of X-ray spectrum (EDAX) of $Co_{0.03M}Fe_{2.97M}O_4$ nanoparticles

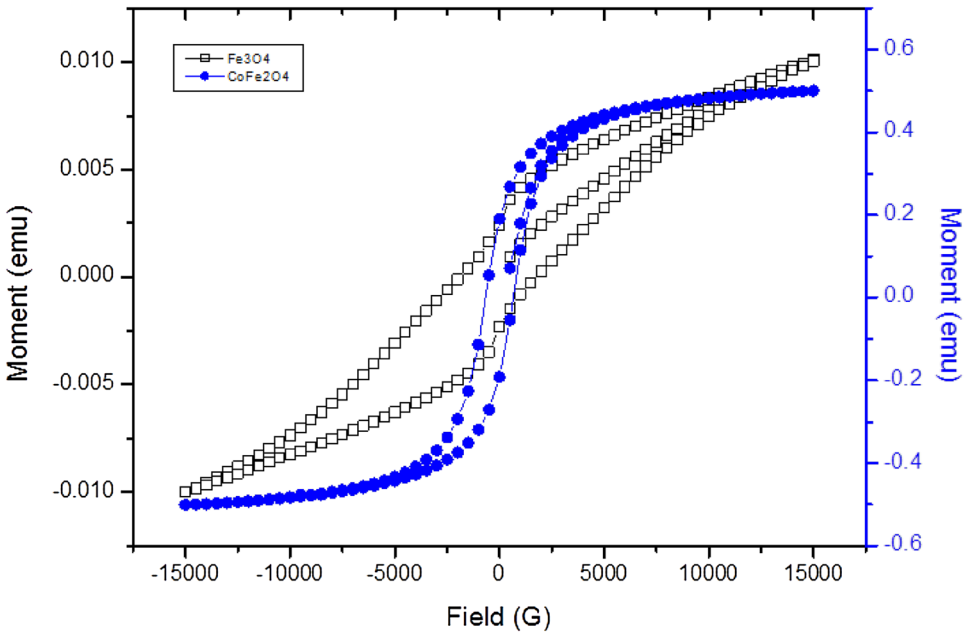

Fig. 5 VSM images of Fe_3O_4 and $Co_{0.03M}Fe_{2.97M}O_4$ nanoparticles at room temperature

Table 4 VSM analysis of Fe_3O_4 and $Co_{0.03M}Fe_{2.97M}O_4$ samples

Sample	M_s (emu/g)	M_r (emu/g)	H_{ci} (G)	Magnetic moment (μB)	$R = M_r/M_s$	Anisotropy constant (K) erg/g
$Fe_{3M}o_4$	10.064E–3	2.3715E–3	1817.7	4.34×10^{-4}	0.2356	19.05
$Co_{0.03M}Fe_{2.97M}O_4$	0.5008	0.1908	661.04	0.0210	0.3809	344.84

among tetrahedral and octahedral voids which defines the antiparallel magnetic spin enclosed by the tetrahedral along with octahedral sites. It causes inverse spinel ferromagnetic structure. The following reduction in saturation magnetization is a way of decreasing the particle size. The highest coercive field up to 661.04 G is accredited to the sample synthesized at pH ~ 11 [37]. The sharing of cations among the lattice sites is provisional on methodologies of preparation. The average particle size is very small (9 nm) and approaches the simple dimension of a simple saturated magnetic domain. The setback of magnetization can occur only by complete rotation of domain within a particle. From Table 4, the coercivity is decreased when Co^{2+} is increased and then the magnetic specifications considerably increased. Because Fe^{3+} ions are parallel to one direction and remaining half of the Fe^{3+} ions parallel to opposite direction, and hence they cancel each other. Therefore, the net magnetic moment is only due to Fe^{3+} ions alone. The magnetic moment (μB) per atom in Bohr magneton for each sample is calculated using the following equation and included in Table 4:

$$\mu B = M \times \left[M_S/5585\right]$$

where 'M' is the molecular weight of $CoFe_2O_4$ [38]. For lower value of magnetic moment was obtained of all sample exhibits to minimize energy loss. The remnant ratio is a property of magnetic materials results high value, the lower value of remnant to help us to analyze different materials response and accordingly determine where the materials to be applied. The lesser remnant ratio was used as the sensitivity, whereas higher values of remnant ratio designate different materials response of magnetic recording and memory devices. Also the magnetic anisotropy (K) is calculated as [39]

$$K = \left(H_{ci} \times M_s\right)/0.96\ \text{erg/g}$$

Magnetic anisotropy depends upon the magnetic properties. It gives some valuable information about the orientation of the field with respect to the crystal lattice. From Table 4, magnetic anisotropy increases (19.05 → 344.84 erg/g) when Co is added with Fe_3O_4. This is due to the fact that Hc decreases with increase in magnetocrystalline anisotropy [39]. The hysteresis loop is very narrow, so the loop area is less. Hence, hysteresis loss is minimum where as coercivity and retentivity are small, having low eddy current loss results all samples are exhibited to soft magnetic materials. This is the important consideration when the materials can be used for microwave frequency applications.

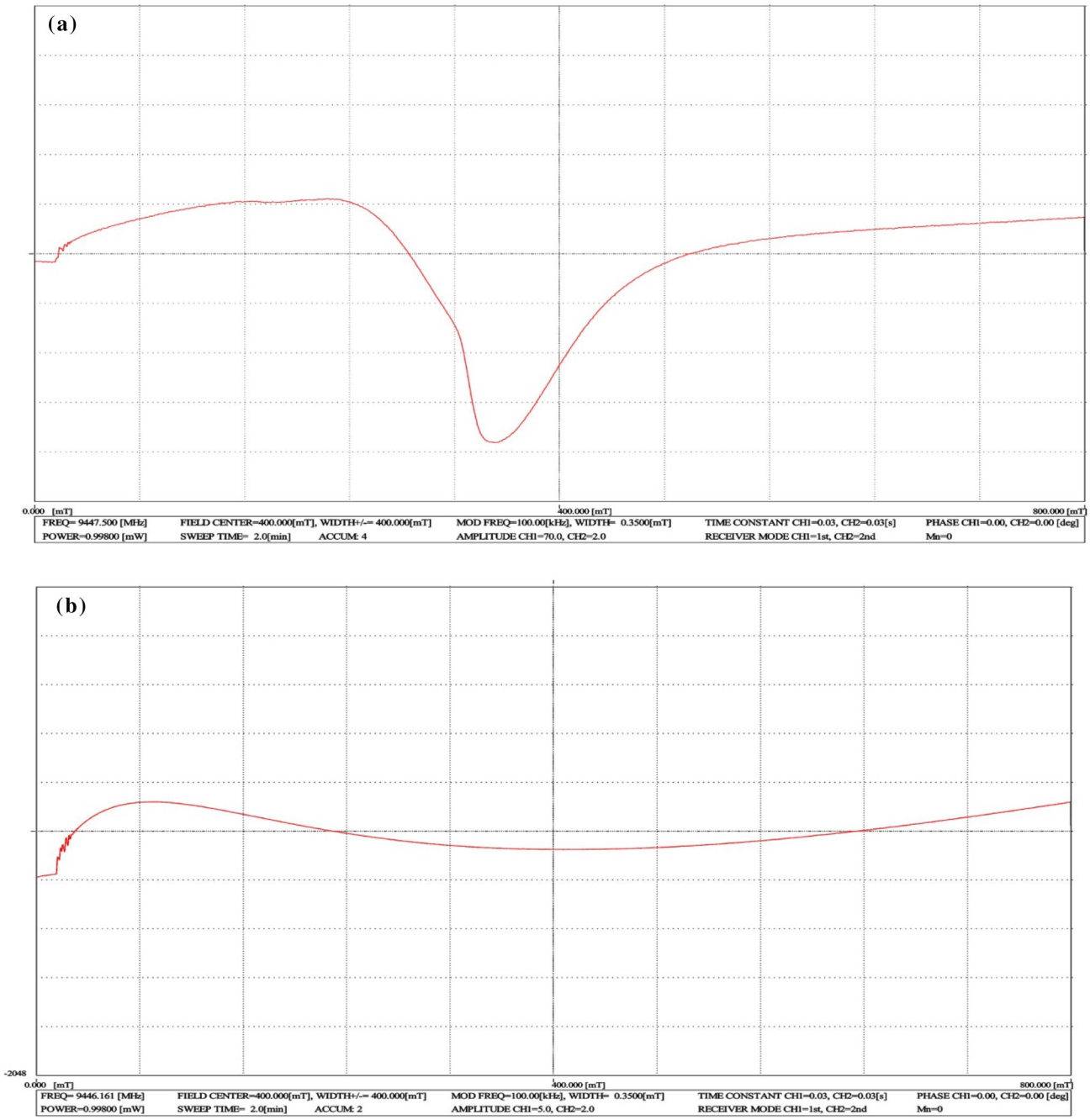

Fig. 6 EPR images of **a** $Fe_{3M}O_4$ and **b** $Co_{0.03M}Fe_{2.97M}O_4$ nanoparticles at room temperature

3.5 EPR analysis

Electron spin resonance (ESR) spectra also called electron paramagnetic resonance (EPR) spectra had confined to the evaluation of molecules or ions having more unpaired electrons. Still, the technique is used for investigating the character of aspect in paramagnetic systems. It is same as the frequency split-up among two voids. This forms the basis of resonance phenomenon. It has been used to study of radical atoms with at least one unpaired electron formed in the materials. Since the radicals characteristically yield an unpaired spin on the ferrite particles from which electron is uninvolved. On the other hand, the materials normally have an oxygen molecule O^{2-} that missed an electron and will steady it by thieving an electron from an adjacent molecule (Co^{2+}, Fe^{3+}). It is particularly fruitful that the radicals have been produced in the materials. The study of radicals gives

selective information about the locations of cations and magnetic specifications. The g factor was calculated using the following equation [38, 40]:

$$g = h\nu/H\beta$$

where (h) is the Planck's constant, ν is the frequency; H is the resonance magnetic field and β is the Bohr magnetron. The EPR spectra of $Co_xFe_{3-x}O_4$ (where $x = 0.03$ M) are shown in Fig. 6. The strong dipole interactions give g value and a huge resonance line width, while strong super-exchange interactions produce a small line width and g value ($g = 2.40$). This suggests that the magnetic particle spins interact with O^{2-}. Hence, magnetic materials exhibit to ferromagnetism as the result of unpaired electrons spins can be induced between tetrahedral and octahedral sites. Generally, the magnetic dipolar interactions and super-exchange interactions between the magnetic ions through oxygen ions are the two important factors that determine the g values and the resonance line width (H). The super-exchange interactions generally increase, when the distance between the magnetic ions and oxygen ions decreases. From the EPR spectra, all the samples display a sharp symmetrical signal and a broad asymmetrical signal with a slight shift from the free electron position ($g = 2.0023$). The ferromagnetic behavior of the samples is confirmed through the g values ($g = 2.812$). The line width and the g values obtained for the samples may be attributed to the ferromagnetic resonance due to Co^{2+} ions [41].

4 Conclusions

The PVP-coated cubic inverse spinel cobalt ferrite nanoparticles were acquired by chemical co-precipitation technique. XRD results show that the particle sizes fall in the range from 19 to 5 nm. The FT–IR spectroscopy expresses the relative occupancy between half of Co^{2+} ions in the tetrahedral along with octahedral fashion through their lower and higher vibration modes. So these materials behaved as ferromagnetic materials about the inverse spinel structure of the cobalt ferrite. The TEM is exposed to a good formation of agglomerated spherical nanosphere. EDX confirmed the occurrence of Co, Fe, C, O elements alone in the sample. The VSM results reveal that the hysteresis loop of the samples was disturbed by doped Co^{2+} at the room temperature, resulting in the increase of exchange interaction connecting two sites. The EPR spectra at room temperature confirm the occurrence of ferromagnetism from the g value of Co-doped Fe_3O_4 nanoparticles.

Acknowledgements We remain grateful to the Administration of St. Joseph's College of Arts & Science (Autonomous), Cuddalore, Tamil Nadu, India, for providing the 'Research Lab for Nanotechnology and Crystal growth' laboratory for synthesis of nanomaterials in our work. And the authors are indebted to PG & Research Department of Physics, Arignar Anna Govt Arts College, Villupuram, for proving laboratory facility.

Compliance with ethical standards

Conflicts of interest There are no conflicts to declare.

References

1. Dippong T, Levei EA, Cadar O, Mesaros A, Borodi G (2017) Sol-gel synthesis of $CoFe_2O_4$:SiO_2 nanocomposites—insights into the thermal decomposition process of precursors. J Anal Appl Pyrolysis 125:169–177. https://doi.org/10.1016/j.jaap.2017.04.005
2. Dippong T, Levei EA, Cadar O, Goga F, Barbu-Tudoran L, Borodi G (2017) Size and shape-controlled synthesis and characterization of $CoFe_2O_4$ nanoparticles embedded in a PVA-SiO_2 hybrid matrix. J Anal Appl Pyrolysis 128:121–130. https://doi.org/10.1016/j.jaap.2017.10.018
3. Dipponga T, Cadarb O, Leveib EA, Deacc IG, Diamandescud L, Barbu-Tudoran L (2018) Influence of cobalt ferrite content on the structure and magnetic properties of (CoFe2O4)X (SiO2-PVA)100-X nanocomposites. Ceram Int 44:7891–7901. https://doi.org/10.1016/j.ceramint.2018.01.226
4. Dippong T, Cadar O, Levei EA, Bibicu I, Diamandescu L, Leostean C, Lazar M, Borodi G, Tudoran Lucian Barbu (2017) Structure and magnetic properties of $CoFe_2O_4$/SiO_2 nanocomposites obtained by sol-gel and post annealing pathways. Ceram Int 43:2113–2122. https://doi.org/10.1016/j.ceramint.2016.10.192
5. Kiran VS, Sumathi S (2017) Comparison of catalytic activity of bismuth substituted cobalt ferrite nanoparticles synthesized by combustion and co- precipitation method. J Magn Magn Mater 421:113–119. https://doi.org/10.1016/J.Jmmm.2016.07.068
6. Zeb F, Sarwer W, Nadeem K, Kamran M, Mumtaz M, Krenn H, Letofsky-Papst I (2016) Surface spin- glass in cobalt ferrite nanoparticles dispersed in silica matrix. J Magn Magn Mater 407:241–246. https://doi.org/10.1016/j.jmmm.2016.01.084
7. Heiba ZK, Mohamed MB, Ahamed SI (2017) Cation distribution correlated with magnetic properties of cobalt ferrite nanoparticles defective by vanadium doping. J Magn Magn Mater 441:409–416. https://doi.org/10.1016/j.jmmm.2017.06
8. Maurya JC, Janrao PS, Datar AA, Kanhe NS, Bhoraskar SV, Mathe VL (2016) Evidence of domain wall pinning in aluminum substituted cobalt ferrites. J Magn Magn Mater 412:164–171. https://doi.org/10.1016/j.jmmm.2016.03.074
9. Sontu UB, Yelasani V, Musugu VRR (2015) Structural, electrical and magnetic characteristics of nickel substituted cobalt ferrite nano particles, synthesized by self combustion method. J Magn Magn Mater 374:376–380. https://doi.org/10.1016/j.jmmm.2014.08.072
10. Dippong Thomas, Levei EA, Diamandescu L, Bibicu I, Leostean C, Borodi G, Tudoran LB (2015) Structural and magnetic properties of CoxFe3– xO4 versus Co/Fe molar ratio. J Magn Magn Mater 394:111–116. https://doi.org/10.1016/j.jmmm.2015.06.055
11. Dippong T, Levei EA, Tanaselia C, Gabor M, Nasui M, Tudoran LB, Borodi G (2016) Magnetic properties evolution of the CoxFe3-xO4/SiO2 system due to advanced thermal treatment

at 700 °C and 1000 °C. J Magn Magn Mater 410:47–54. https://doi.org/10.1016/j.jmmm.2016.03.020
12. Khaja Mohaideen K, Joy PA (2013) Influence of initial particle size on the magnetostriction of sintered cobalt ferrite derived from nanocrystalline powders. J Magn Magn Mater 346:96–102. https://doi.org/10.1016/j.jmmm.2013.07.016
13. Babu KR, Rao KR, Babu BR (2017) Cu^{2+} modified physical properties of Cobalt- Nickel ferrites. J Magn Magn Mater 434:118–125. https://doi.org/10.1016/j.jmmm.2017.03.044
14. Biswal D, Peeples BN, Peeples C, Pradhan AK (2013) Tuning of magnetic properties in cobalt ferrite by varying Fe^{+2} and Co^{+2} molar ratios. J Magn Magn Mater 345:1–6. https://doi.org/10.1016/j.jmmm.2013.05.052
15. Kooti M, Saiahi S, Motamedi H (2013) Fabrication of silver-coated cobalt ferrite nanocomposite and the study of its antibacterial activity. J Magn Magn Mater 333:138–143. https://doi.org/10.1016/j.jmmm.2012.12.038
16. Abbas YM, Mansour SA, Ibrahim MH, Ali SE (2011) Microstructure characterization and cation distribution of nanocrystalline cobalt ferrite. J Magn Magn Mater 323:2748–2756. https://doi.org/10.1016/j.jmmm.2011.05.038
17. Abbas YM, Mansour SA, Ibrahim MH, Ali SE (2012) Structural and magnetic properties of nanocrystalline stannic substituted cobalt ferrite. J Magn Magn Mater 324:2781–2787. https://doi.org/10.1016/j.jmmm.2012.04.010
18. Ahmad R, Gul IH, Zarrar M, Anwar H, khan Niazi MB, Khan A (2016) Improved electrical properties of cadmium substituted cobalt ferrites nanoparticles for microwave application. J Magn Magn Mater 405:28–35. https://doi.org/10.1016/j.jmmm.2015.12.019
19. Amirabadizadeh A, Salighe Z, Sarhaddi R, Lotfollahi Z (2017) Synthesis of ferrofluids based on cobalt ferrite nanoparticles: Influence of reaction time on structural, morphological and magnetic properties. J Magn Magn Mater 434:78–85. https://doi.org/10.1016/j.jmmm.2017.03.023
20. Sagayaraj R, Aravazhi S, Praveen P, Chandrasekaran G (2018) Structural, morphological and magnetic characters of PVP coated ZnFe2O4 nanoparticles. J Mater Sci Mater Electron 29:2151. https://doi.org/10.1007/s10854-017-8127-4
21. Kairimi Z, Mohammadifar Y, Shokrollahi H, Khameneh Asl Sh, Yousefi Gh, Karimi L (2014) Magnetic and structural properties of nano sized Dy –doped cobalt ferrite synthesized by co-precipitation. J Magn Magn Mater 361:150–156. https://doi.org/10.1016/j.jmmm.2014.01.016
22. Avazpour L, Zandi khajeh MA, Toroghinejad MR, Shokrollahi H (2015) Synthesis of single-phase cobalt ferrite nanoparticles via a novel EDTA/EG precursor-based route and their magnetic properties. J Alloys Compd 637:497–503. https://doi.org/10.1016/j.jallcom.2015.03.041
23. Nlebedim IC, Synder JE, Moses AJ, Jiles DC (2010) Dependence of the magnetic and magnetoelastic properties of cobalt ferrite on processing parameters. J Magn Magn Mater 322:3938–3942. https://doi.org/10.1016/j.jmmm.2010.08.026
24. Dey C, Baishya K, Ghosh A, Goswami MM, Ghosh A, Mandal K (2017) Improvement of drug delivery by hyperthermia treatment using magnetic cubic cobalt ferrite nanoparticles. J Magn Magn Mater 427:168–174. https://doi.org/10.1016/j.jmmm.2016.11.024
25. Chndra G, Srivastava RC, Reddy VR, Agarwal HM (2017) Effect of sintering temperature on magnetization and mossbauer parameters of cobalt ferrite nanoparticles. J Magn Magn Mater 427:225–229. https://doi.org/10.1016/j.jmmm.2016.10.082
26. Prabhakaran T, Hemalatha J (2014) Chemical control on the size and properties of nano NiFe2O4 synthesized by sol–gel autocombustion method. Ceram Int 40:3315–3324. https://doi.org/10.1016/j.ceramint.2013.09.103
27. Nadeem K, Zeb F, Abid MA, Mumtaz M, Rehman MA (2014) Effect of amorphous silica matrix on structural, magnetic, and dielectric properties of cobalt ferrite/silica nanocomposites. J Non-Cryst Solids 400:45–50. https://doi.org/10.1016/j.jnoncrysol.2014.05.004
28. Sridhar R, Ravinder D, Kumar KV (2012) Synthesis and characterization of copper substituted nickel nano-ferrites by citrate-gel technique. Adv Mater Phys Chem 2:192–199. https://doi.org/10.4236/ampc.2012.23029
29. Kumar GR, Kumar KV, Venudhar YC (2012) Synthesis, structural and magnetic properties of copper substituted nickel ferrites by sol–gel method. Mater Sci Appl 3:87–91. https://doi.org/10.4236/msa.2012.32013
30. Hankare PP, Sanadi KR, Pandav RS, Patil NM, Garadkar KM, Mulla IS (2012) Structural, electrical and magnetic properties of cadmium substituted copper ferrite by sol–gel method. J Alloys Compd 540:290–296. https://doi.org/10.1016/j.jallcom.2012.06.018
31. Batoo KM, El-sadek M-SA (2013) Electrical and magnetic transport properties of Ni–Cu–Mg ferrite nanoparticles prepared by sol–gel method. J Alloys Compd 566:112–119. https://doi.org/10.1016/j.jallcom.2013.02.129
32. Gharibshahian M, Mirzaee O, Nourbakhsh MS (2017) Evaluation of superparamagnetic and biocompatible properties of mesoporous silica coated cobalt ferrite nanoparticles synthesized via microwave modified Pechini method. J Magn Magn Mater 425:48–56. https://doi.org/10.1016/j.jmmm.2016.10.116
33. Ghasemi A, Ekhlasi S, Mousavinia M (2014) Effect of Cr and Al substitution cations on the structural and magnetic properties of Ni0.6Zn0.4Fe2−xCrx/2Alx/2O4 nanoparticles synthesized using the sol–gel auto-combustion method. J Magn Magn Mater 354:136–145. https://doi.org/10.1016/j.jmmm.2013.10.022
34. Sivakumar P, Ramesh R, Ramanand A, Ponnusamy S, Muthamizhchelvan C (2012) Synthesis, studies and growth mechanism of ferromagnetic NiFe2O4 nanosheet. Appl Surf Sci 258(2012):6648–6652. https://doi.org/10.1016/j.apsusc.2012.03.099
35. Ansari F, Sobhani A, Salavati-Niasari M (2016) Facile synthesis, characterization and magnetic property of CuFe12O19 nanostructures via a sol–gel auto-combustion process. J Magn Magn Mater 401:362–369. https://doi.org/10.1016/j.jmmm.2015.10.049
36. Nikumbh AK, Pawar RA, Nighot DV, Gugale GS, Sangale MD, Khanvilkar MB, Nagawade AV (2014) Structural, electrical, magnetic and dielectric properties of rare-earth substituted cobalt ferrites nanoparticles synthesized by the co-precipitation method. J Magn Magn Mater 355:201–209. https://doi.org/10.1016/j.jmmm.2013.11.052
37. Iwaizumi M, Tachibana M, Tero-Kubota S (1987) EPR studies of copper(II) and cobalt(II) complexes of adriamycin. J Inorg Biochem 30:133. https://doi.org/10.1016/0162-0134(87)80049-1
38. Sagayaraj R, Aravazhi S, Chandrasekaran G (2018) Synthesis, spectroscopy, and magnetic characterizations of PVP-assisted nanoscale particle. J Supercond Nov Magn 31:603. https://doi.org/10.1007/s10948-018-4593-z
39. Moradmard H, Shayesteh SF, Tohidi P, Abbas Z, Khaleghi M (2015) Structural, magnetic and dielectric properties of magnesium doped nickel ferrite nanoparticles. J Alloys Compd 650:116. https://doi.org/10.1016/j.jallcom.2015.07.269

40. Kavas H, Kasapoğlu N, Baykal A et al (2009) Characterization of $NiFe_2O_4$ nanoparticles synthesized by various methods. Chem Pap 63:450. https://doi.org/10.2478/s11696-009-0034-6
41. Elilarassi R, Chandrasekaran G (2017) Influence of nickel doping on the structural, optical and magnetic properties of TiO2 diluted magnetic semiconductor nanoparticles prepared by high energy ball-milling technique. J Mater Sci Mater Electron 28:14536–14542. https://doi.org/10.1007/s10854-017-7317-4